ACCOUNTS of chemical research

Article

pubs.acs.org/accounts

Toward Molecular Catalysts by Computer

Simone Raugei,* Daniel L. DuBois, Roger Rousseau,* Shentan Chen, Ming-Hsun Ho, R. Morris Bullock, and Michel Dupuis*

Center for Molecular Electrocatalysis, Physical Sciences Division, Pacific Northwest National Laboratory, Richland, Washington 99352, United States

CONSPECTUS: Rational design of molecular catalysts requires a systematic approach to designing ligands with specific functionality and precisely tailored electronic and steric properties. It then becomes possible to devise computer protocols to design catalysts by computer. In this Account, we first review how thermodynamic properties such as redox potentials ($E°$), acidity constants (pK_a), and hydride donor abilities (ΔG_{H^-}) form the basis for a framework for the systematic design of molecular catalysts for reactions that are critical for a secure energy future. We illustrate this for hydrogen evolution and oxidation, oxygen reduction, and CO conversion, and we give references to other instances where it has been successfully applied. The framework is amenable to quantum-chemical calculations and conducive to predictions by computer. We review how density functional theory allows the determination and prediction of these thermodynamic properties within an accuracy relevant to experimentalists (~0.06 eV for redox potentials, ~1 pK_a unit for pK_a values, and 1−2 kcal/mol for hydricities). Computation yielded correlations among thermodynamic properties as they reflect the electron population in the d shell of the metal center, thus substantiating empirical correlations used by experimentalists. These correlations point to the key role of redox potentials and other properties (pK_a of the parent aminium for the proton-relay-based catalysts designed in our laboratory) that are easily accessible experimentally or computationally in reducing the parameter space for design. These properties suffice to fully determine free energies maps and profiles associated with catalytic cycles, i.e., the relative energies of intermediates. Their prediction puts us in a position to distinguish a priori between desirable and undesirable pathways and mechanisms. Efficient catalysts have flat free energy profiles that avoid high activation barriers due to low- and high-energy intermediates. The criterion of a flat energy profile can be mathematically resolved in a functional in the reduced parameter space that can be efficaciously calculated by means of the correlation expressions. Optimization of the functional permits the *prediction by computer* of design points for optimum catalysts. Specifically, the optimization yields the values of the thermodynamic properties for efficient (high rate and low overpotential) catalysts. We are on the verge of design of molecular electrocatalysts by computer. Future efforts must focus on identifying actual ligands that possess these properties. We believe that this can also be achieved through computation, using Taft-like relationships linking molecular composition and structure with electron-donating ability and steric effects. We note also that the approach adopted here of using free energy maps to decipher catalytic pathways and mechanisms does not account for kinetic barriers associated with elementary steps along the catalytic pathway, which may make thermodynamically accessible intermediates kinetically inaccessible. Such an extension of the approach will require further computations that, however, can take advantage of Polanyi-like linear free energy relationships linking activation barriers and reaction free energies.

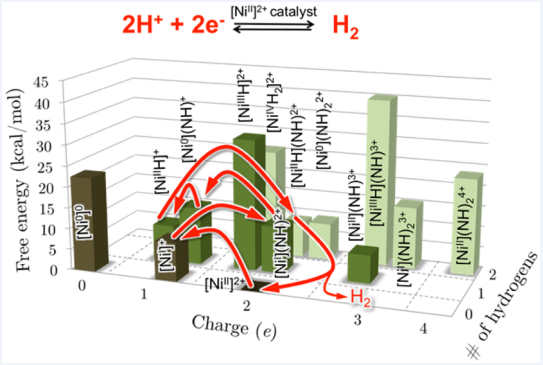

INTRODUCTION

It is recognized that a notable advantage of molecular catalysis is the ability to tune ligand design to create complexes with exquisitely tailored catalytic properties and performances.[1] With design principles in hand (ligand composition and structure), it is possible to use quantum molecular computations to systematically assess and predict the effects associated with changes in electronic structure (electron-withdrawing or -donating abilities) and steric characteristics of the ligands. To this end, it is necessary to have a carefully benchmarked level of electronic structure theory that possesses a useful level of accuracy, perhaps "chemical" accuracy.[2−4] Modern density functional theory (DFT) is often successful in this regard for classes of molecules for which specific functionals of the density prove satisfactory. Examples of successes of this type are numerous in the literature.

Computations with "chemical" accuracy across different properties (e.g., redox potentials and acidity constants) are even more challenging but also more powerful: they enable viable sequences of elementary steps from reactants to products to be ascertained. For example, production of H_2, an important process in energy science, is a "simple" two-proton, two-electron reaction, yet it has considerable complexity introduced

Received: September 16, 2014
Published: January 9, 2015

DOI: 10.1021/ar500342g
Acc. Chem. Res. 2015, 48, 248−255

by the order of delivery of protons and electrons. Calculations[5,6] are able to *rationalize* how the sequence of reduction and protonation steps depends on the reaction conditions (pH and applied potential). Great insights can already be gleaned from such analyses, as the concept and approach are applicable to reactions that involve a greater number of protons and electrons.

In this Account, we go a step further: we *extract design points* from our computations. We leverage accurate thermodynamic property predictions and the concept of a flat energy profile along a catalytic cycle to predict intrinsic characteristics (i.e., turnover frequencies and overpotentials)[7] of efficient electrocatalysts.[8] *We are on the verge of design by computer*. Realizing this goal requires identifying by computer actual ligands that possess these properties. Computed Taft-like relationships linking molecular composition and structure with electron-donating ability and steric effects[9] will provide this path forward.

BACKGROUND

Electrocatalysts based on inexpensive and abundant metals[10,11] that rapidly and efficiently interconvert electrical energy and fuels are envisioned to play a critical role in renewable energy utilization systems.[12−14] A general concept for the development of efficient catalysts is depicted in Figure 1, which represents an

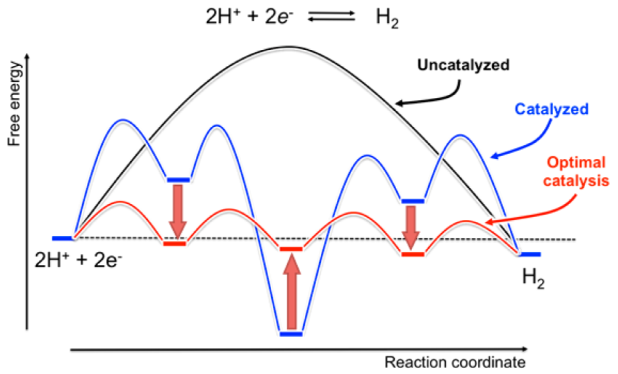

Figure 1. Typical energy profiles for a model reaction that is uncatalyzed (black) or catalyzed (blue and red). The red (up/down) arrows indicate improvement of the catalyst to avoid low- and high-energy intermediates, yielding a relatively flat free energy profile. The red profile is for the more efficient catalyst.

uncatalyzed reaction (black), a catalyzed reaction (blue), and a more efficiently catalyzed reaction (red) that avoids high energy barriers arising from low- or high-energy intermediates.

The realization that many reactions, such as CO_2 reduction, H_2 oxidation and production, O_2 reduction, H_2O oxidation, and N_2 reduction, involve electrons, protons, and hydrides prompted us to propose a thermodynamic framework for the systematic design of catalysts.[1,15] In this framework, the relative free energies of intermediates in the catalytic cycles directly come out from thermodynamic properties such as acidity constants (pK_a), redox potentials ($E°$), and hydride donor abilities (hydricities, ΔG_{H^-}), as illustrated for H_2 oxidation in Scheme 1 and Figure 2.

These thermodynamic properties are, however, not independent.[16−21] They are connected through elementary thermodynamic cycles as shown in Figure 2. In any case, the simple knowledge of the thermodynamic properties allows the prediction of complete free energy maps and free energy

Scheme 1. Key Intermediates in the Oxidation of H_2 by a Ni^{II} Catalyst and the Connecting Thermodynamic Quantities (Hydride Donor Ability, Redox Potentials, and Acidity Constant)

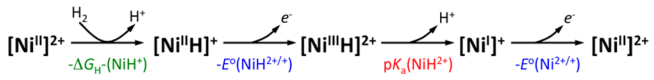

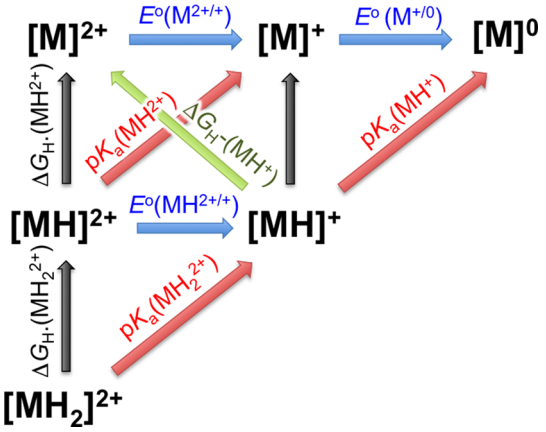

Figure 2. Possible intermediates and connecting thermodynamic transformations for a H_2 production/oxidation catalyst (Scheme 1): redox potentials ($E°$, blue), acidity constants (pK_a, red), hydricities (ΔG_{H^-}, green), and homolytic bond dissociation energies ($\Delta G_{H\cdot}$, black). Horizontal axis = redox states; vertical axis = hydrogen atom transfers; diagonals = proton/hydride transfers.

profiles. The catalytic mechanism corresponds to the pathway with the "flattest" free energy profile.

The thermodynamic diagram in Figure 2 has a significantly more complicated appearance when functional groups (acting as "proton relays") in the second coordination sphere of the metal center are present.[1,5,6,22−26] The relays may be in non-protonated or protonated states. Examples of such more complicated diagrams have been fully described in ref 6.

In other cases, the substrate undergoing the chemical transformation binds a proton. It may also bind a hydrogen atom, giving rise to a change in oxidation state. Scheme 2

Scheme 2. Key Intermediates in a Four-Proton, Four-Electron Reduction of O_2 by Fe^{III} Porphyrin Catalysts [Fe^{III}] with the Connecting Thermodynamic Transformations Depicted in Figure 3

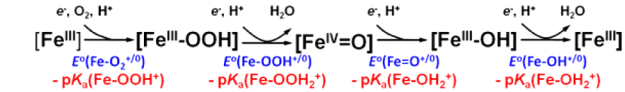

depicts selected intermediates in the reduction of O_2 to H_2O,[25,26] while Scheme 3 illustrates intermediates in the reduction of CO to methanol in metal carbonyl complexes.[27] They differ from Scheme 1 in that the protons bind to the

Scheme 3. Key Intermediates in the Conversion of CO to methanol in Metal Carbonyls[27] with the Connecting Thermodynamic Transformations Depicted in Figure 4

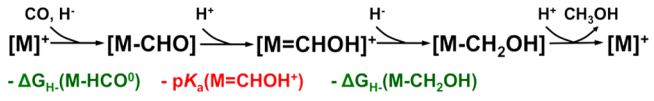

DOI: 10.1021/ar500342g
Acc. Chem. Res. 2015, 48, 248−255

substrate molecules (O_2 and CO, respectively) coordinated to the metal center. Nevertheless, the elementary transformations connecting all of the reaction intermediates involve pK_a's, redox potentials, and hydride donor abilities (Figures 3 and 4).

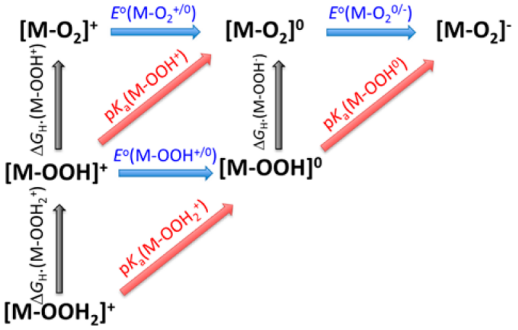

Figure 3. Possible intermediates and connecting thermodynamic transformations for an O_2 reduction catalyst (Scheme 2).

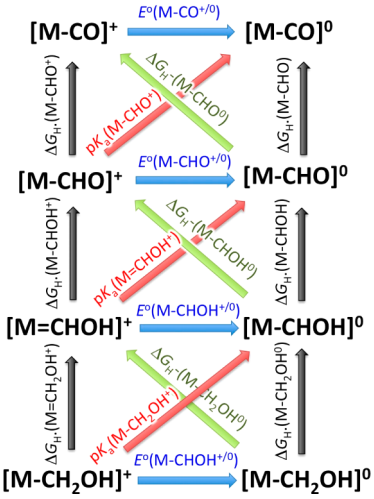

Figure 4. Possible intermediates and connecting thermodynamic transformations for the conversion of CO to HCOH (Scheme 3).

The transformations depicted in simple forms in Schemes 1−3 and Figures 2−4 are indicative of *a general and powerful framework*. This framework has been successfully applied in the development of Ni-based molecular electrocatalysts for H_2 oxidation and production[6,28] and formate oxidation,[12−15,29] rhenium-based complexes for the reduction of CO,[27] and, currently, for the development of iron porphyrin complexes for the reduction to O_2 to H_2O.[25,26] The same framework has also formed the basis for the development of stoichiometric hydride transfer reactions from rhodium and cobalt hydrides to boron-containing molecules to form borohydrides[30,31] and from nickel and platinum hydrides to metal carbonyl complexes to generate formyl complexes.[32] All of these catalytic and stoichiometric reactions are potentially important for electrical energy storage and conversion technologies.

The framework is amenable to quantum-chemical calculations[5,6] *and conducive to predictions by computer.* This is the focus of this Account. We first review briefly the computational methodology that permits the accurate predictions of the thermodynamic properties of interest.[5,6] We then highlight how the prediction of the properties enables differentiation between possible catalytic pathways that differ only in the sequence of elementary steps, eliminating those that give rise to large energy barriers.[6] We note that the approach highlighted below does not account for kinetic barriers, which may make thermodynamically accessible minima kinetically inaccessible. We then show how we can make predictions about the values that these properties must have in an efficient catalyst. We end the Account by discussing our path forward to complete the design of molecular catalysts by computer.

COMPUTATIONAL METHODOLOGY

The use of computation to predict thermodynamic properties and to establish a priori free energy maps and free energy profiles sets upper limits on the accuracy of the calculations. On the basis of our experience, to usefully inform experimentalists it is necessary to determine pK_a's within 1 pK_a unit, redox potentials within 50 mV, and hydride donor abilities within 1−2 kcal/mol. These values are consistent with so-called "chemical" accuracy (i.e., 1 kcal/mol) put forth by theoreticians for the development of quantum-mechanical methods[2,3] and with typical experimental accuracies achievable for these quantities.

For these studies, we expounded on the work of Qi et al.[33,34] and established a protocol yielding thermodynamic properties with the required accuracy. The level of theory for the calculations[5,6,35] included a hybrid exchange−correlation functional of the density, a composite basis set, and a description of solvation via the polarizable continuum model. We adopted a protocol based on isodesmic reactions[36] whereby one or a few reference complexes are used, and the calculations provide differences in energy with respect to the references (Scheme 4). This is a well-established methodology in which the left- and right-hand sides of the reaction conserve total charge, number of bonds and their types, and redox states.

Scheme 4. Isodesmic Reaction Scheme Used for the Calculation of pK_a Values; Similar Reactions Were Used for Redox Potentials and Hydricities[5,6]

$$[HNiL_n]^+ \rightleftharpoons NiL_n + H^+ \qquad +1.364pK_a$$

$$^{Ref}NiL_n + H^+ \rightleftharpoons {}^{Ref}[HNiL_n]^+ \qquad -1.364pK_a^{Ref}$$

$$[HNiL_n]^+ + {}^{Ref}NiL_n \rightleftharpoons NiL_n + {}^{Ref}[HNiL_n]^+ \qquad +\Delta_rG^\circ$$

$$pK_a = \Delta_rG^\circ/1.364 + pK_a^{Ref}$$

Under isodesmic conditions, calculated differences in energy benefit from cancellations of systematic errors. This is borne out by our findings[5,6] where linear correlations (theory vs experiment) were found for a training set of Ni(diphosphine)$_2$ complexes (hereafter denoted as $[Ni(P_2)_2]^{2+}$). We note that the intercepts of those correlations are located at the origin and that the slopes are near unity, with mean absolute errors for the various properties within the above limits.[5,6]

THERMODYNAMIC DIAGRAMS BY COMPUTER

Correlations among thermodynamic properties can be extracted from the calculations (Table 1). The findings provide support for empirical correlations often used by experimentalists.[17,37] For example, the pK_a of Ni hydride $[Ni^{II}H^+]$ is directly related to the $E^\circ(Ni^{I/0})$ redox potential and the hydride-donating strength of $[Ni^{II}H^+]$ to the $E^\circ(Ni^{II/I})$ potential. Not surprisingly, both properties depend on the

DOI: 10.1021/ar500342g
Acc. Chem. Res. 2015, 48, 248−255

Table 1. Correlations among Thermodynamic Properties for a Set of $[Ni(P_2)_2]^{2+}$ Catalysts[4,5] In Acetonitrile Solution That Allow the Construction of Full Thermodynamic Diagrams As in Figure 2 for This Class of Catalysts[a]

Thermodynamic Correlations for $[Ni(P_2)_2]^{2+}$ complexes						
$\Delta G°_H$-($Ni^{II}H^+$)	=	+	21.72	$E^0(Ni^{II/I})$	+	79.27
$pK_a(Ni^{II}H^+)$	=	-	18.01	$E°(Ni^{I/0})$	-	0.89
$E°(Ni^{III/II}H^{2+/+})$	=	+	1.02	$E°(Ni^{I/0})$	+	1.60
$pK_a(Ni^{III}H^{2+})$	=	-	18.38	$E°(Ni^{I/0})$	-	27.82
$pK_a(Ni^{IV}(H)_2^{3+})$	=	-	16.90	$E°(Ni^{I/0})$	-	24.78
$\Delta G°_H$.($Ni^{II}H^+$)	=	-	1.34	$E°(Ni^{II/I})$	+	53.27
$\Delta G°_H$.($Ni^{III}H^{2+}$)	=	- +	25.05 23.06	$E°(Ni^{I/0})$ $E^0(Ni^{II/I})$	+	15.65
$\Delta G°_H$.($Ni^{IV}(H)_2^{3+}$)	=	+	0.47	$E°(Ni^{I/0})$	+	56.70

[a]All properties are functions of $E°(Ni^{I/0})$ and $E°(Ni^{II/I})$ only. Units are pK_a for pK_a's, eV for $E°$'s, and kcal/mol for hydride donor abilities.

electron density in the d shell of the Ni center as the redox potentials do.

Pendant amines in the second coordination sphere of the metal center in $[Ni(P_2N_2)_2]^{2+}$ catalysts (see Figure 5) act as proton relays and greatly accelerate catalysis while reducing overpotentials. Correlations among thermodynamic properties similar to those discussed earlier exist for catalysts bearing pendant amines. Additional calculations indicate that, remarkably, pendant amines affect the thermodynamic properties by nearly constant shifts (i.e., 1 pK_a unit for $pK_a(M^{II}H^+)$ and 2 kcal/mol for $\Delta G^0{}_H{}^-(M^{II}H^+)$). We assign the shifts to the interactions of the lone-pair electrons of the pendant amine with the d electrons of the metal center.

The pendant amines can accept and deliver protons to the metal center or to an exogenous base. The acidity of the pendant amine is a key factor in the efficacy of proton relays. The acidity of a pendant amine in a complex is closely related to that of the parent aminium. Its pK_a value in the complex is given by a simple expression as shown in Scheme 5, where we note the contribution from $E°(Ni^{I/0})$ as a consequence of the interaction with the metal/ligand core.[6]

Scheme 5. pK_a Value of the Protonated Pendant Amine in a Ni^{II} Complex As a Function of the Acidity of the Parent Aminium; It Depends on the $E°(Ni^{I/0})$ Redox Potential of the Complex, Reflecting the Effects of the d Electrons of

$$pK_a(NH^+)_{Ni(II)} = 0.8\ pK_a(\text{parent aminium}) - 6.8\ E°(Ni^{I/0}) - 3.0$$

At this point we are equipped with all of the pieces of information obtained through calculations that are necessary to predict the relative energies of all catalytic intermediates, including those with proton or hydride on the Ni center and proton on the pendant amine (with the exception of the H_2 adduct). We are in a position to predict the most probable catalytic pathway or mechanism, as we now illustrate.

FREE ENERGY MAPS AND PROFILES BY COMPUTER

The ability to predict free energy profiles along catalytic cycles by computer is an extremely powerful capability. In the case of the Ni catalysts shown in Figure 5, the correlations among properties make the free energy profiles and maps dependent

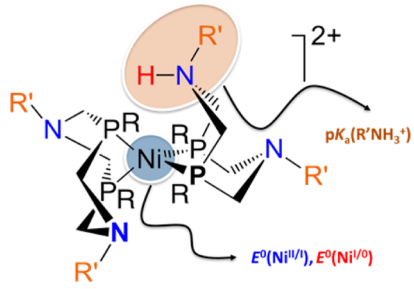

Figure 5. Structure of $[Ni(P^R{}_2N^{R'}{}_2)_2]$ catalysts for H_2 oxidation and production, where $P^R{}_2N^{R'}{}_2$ is the 1,5-R′-3,7-R derivative of 1,5-diaza-3,7-diphosphacyclooctane (R, R′ = aryl, alkyl). Pendant amines acting as proton relays are included in the second coordination sphere of the metal center. The figure illustrates an endo-protonated Ni(I) intermediate. The $E°(Ni^{I/0})$ and $E°(Ni^{II/I})$ redox potentials of Ni and the pK_a of the parent aminium $R'NH_3^+$ suffice to determine completely the thermodynamic diagram for this class of catalysts. See refs 4 and 5.

on *only three parameters* (two redox potentials and the pK_a of the parent aminium), given the electrode potential at which the catalysis runs and the pK_a of the exogenous acid. These three parameters are easily determined experimentally, but in fact, *computation can alleviate the need for experimental measurements.*

Consider the hydrogen production reaction catalyzed by a Ni^{II} catalyst (Scheme 1 in the right-to-left direction). Scheme 1 tells us that two protons and two electrons come together in a succession of steps that end with the formation of the H–H bond. However, it does not tell us the order of the steps, i.e., it does not reveal the mechanism and the pathway of the reaction during catalysis. In contrast, *thermodynamic-property-based diagrams do reveal crucial insights into the mechanism and the pathway*, enabling us to draw the catalytic reaction in the form of a cycle, as shown in Scheme 6 for $[Ni(P_2N_2)_2]^{2+}$ complexes. Figure 6 depicts free energy maps and profiles for this reaction. In the top panel, pillars represent the free energies of intermediates. The taller a pillar, the less desirable and probable is the intermediate.

We analyze first the lowest-energy H_2 production pathway accessible to the simpler $[Ni(P_2)_2]^{2+}$ catalysts (i.e., with no

Scheme 6. Catalytic Cycle for H_2 Production (Counterclockwise) or Hydrogen Oxidation (Clockwise) by a $[Ni^{II}]^{2+}$ Catalyst with Pendant Amines for Alternating Electron Transfer/Proton Transfer Steps (Base and $HBase^+$ Represent the Exogenous Base and Its Conjugate Acid Involved in Proton Delivery)

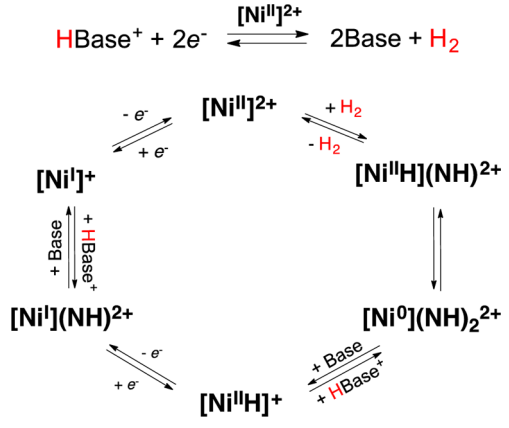

DOI: 10.1021/ar500342g
Acc. Chem. Res. 2015, 48, 248–255

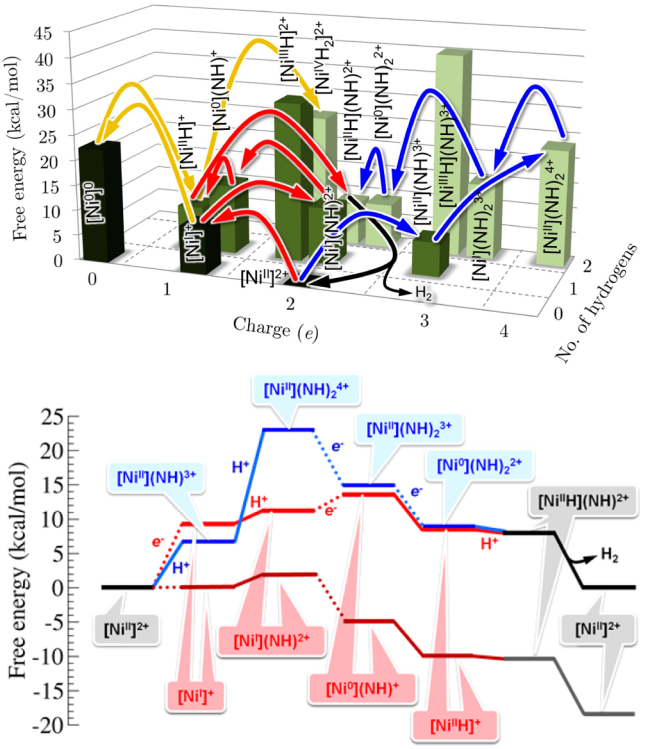

Figure 6. Free energy map and three profiles for H_2 production with the catalyst $[Ni(P^{Ph}{}_2N^{Ph}{}_2)_2]^{2+}$ ($E°(Ni^{II/I})$ = −0.83 V, $E°(Ni^{I/0})$ = −1.02 V, pK_a of parent aminium = 10.6) and protonated dimethylformamide, $(DMF)H^+$ (pK_a = 6.1), in acetonitrile solution under standard conditions (catalyst and $(DMF)H^+$ at 1 M concentration under 1 atm H_2) at an electrode potential equal to the thermodynamic potential for the reaction $2(DMF)H^+ + 2e^- \rightleftarrows 2DMF + H_2$, namely, $V = E°((DMF)H^+/DMF; H_2)$ = −0.386 V (i.e., zero overpotential).[7] (top) Relative free energies of all hydridic and endo-protonated species of the catalytic cycle. The colored arrows correspond to three (out of 12) possible sequences of protonation (P^{loc}, where loc = Ni or N for protonation at Ni or N, respectively)−reduction (E) steps: $EEP^{Ni}P^{Ni}$ (yellow arrows), EP^NEP^N (red arrows), and P^NP^NEE (blue arrows); the black arrows represent the H_2 formation/release step common to all of the pathways. In the $EEP^{Ni}P^{Ni}$ pathway, the formation of H_2 from the Ni^{IV} dihydride has been omitted for clarity. (bottom) Free energy profiles for the EP^NEP^N (red) and P^NP^NEE (blue) sequences at the thermodynamic potential for reduction of protons to H_2 (see refs 4 and 5). The purple curve is the EP^NEP^N profile corresponding to a potential equal to the first reduction potential of $[Ni^{II}]^{2+}$, namely, $E°(Ni^{II/I})$ = −0.83 V. All potentials are with respect to the ferrocenium/ferrocene couple in acetonitrile.

pendant amines; yellow arrows in Figure 6). The high energies of the intermediates $[Ni^0]^0$, $[Ni^{III}H]^+$, and $[Ni^{IV}H_2]^{2+}$ are responsible for large overpotentials and low rates. At the pH value of the solution, protonation of $[Ni^{II}]^{2+}$ or $[Ni^{I}]^+$ is highly endergonic. The initial steps in the catalysis are two one-electron reductions to form the Ni^0 intermediate, which is readily protonated to give $[Ni^{II}H]^+$. The second protonation for H_2 production occurs via the high-energy species $[Ni^{IV}(H)_2]^{2+}$. Introduction of the four pendant amines in the $[Ni(P^{Ph}{}_2N^{Ph}{}_2)_2]^{2+}$ catalysts results in many more possible intermediates and a much more complex free energy landscape, as clearly shown in Figure 6 by the red and blue arrows involving all of the hydride and endo-protonated species (see Figure 5). Here we show only two possible pathways: the red arrows connect the intermediates in the sequence of steps electron−proton−electron−proton (EPEP) followed by H_2 production (black arrows); the blue arrows connect the intermediates in the proton−proton−electron−electron (PPEE) sequence. The corresponding free energy profiles (red for EPEP and blue for PPEE) are shown in the bottom panel of Figure 6.

The sequence of double protonation followed by double reduction (PPEE) is not favorable, as the doubly protonated Ni^{II} intermediate is very high in energy. In contrast, the EPEP sequence is much more facile; in fact, it is the most facile of all of the possible sequences. Alternation of the protonations and reductions has the effect of balancing the charge buildup resulting from the addition of too many electrons or protons. This concept of charge balancing is widely discussed in the literature on proton-coupled electron transfer (PCET).[38,39]

A second point illustrated in Figure 6 is that at the potential of the catalysis[40,41] (the first reduction of $[Ni^{II}]^{2+}$, $V = E°(Ni^{II/I})$), the relative energies of all (six) steps add up to an excess energy of ∼19 kcal/mol that is provided to the reaction via the electrode potential. This is the thermodynamic overpotential (∼0.4 V per electron) for the reaction under the specific operating conditions (electrode potential and pK_a of the exogenous base).

These two points are examples of the insight provided by the free energy map approach that is accessible by a priori computations. We conclude this section noting the conundrum: pendant amines significantly increase the system complexity, yet they are directly responsible for the increase in catalytic activity! They allow protons to be stored on the catalyst, something that is not possible with the simpler $[Ni(P_2)_2]^{2+}$ catalysts. In addition, protonation of the P_2N_2 ligands causes shifts in redox potentials that allow more electrons to be stored on the catalyst at a given potential. The ability to store protons and electrons on the catalyst is the single most important reason for the increased activity of the $[Ni(P_2N_2)_2]^{2+}$ catalysts.

CATALYST DESIGN BY COMPUTER

For optimal catalysis, we need to avoid intermediates with high or low free energies. So far we have shown how computation yields the free energy differences associated with individual steps along a cycle. As a set, these energies are solely dependent on $E°(Ni^{II/I})$ and $E°(Ni^{I/0})$ of the catalyst and the pK_a of the parent aminium. From here, we can go a step further: *we can predict the values of these three parameters for what we say are "optimum" catalysts.*

Mathematically, we can enforce the requirement of small free energy changes in consecutive steps by minimizing the objective function given in eq 1:

$$\chi^2 = \frac{1}{n_{steps}} \sum_{k}^{n_{steps}} |\Delta G_k|^2 \qquad (1)$$

where ΔG_k is the free energy associated with reaction step k and n_{steps} is the number of steps in the catalytic cycle. The minimization must be done for specific "operating conditions" (pK_a of the exogenous acid and applied electrode potential).

An ideal catalyst should operate at the thermodynamic potential dictated by the acidity of the medium, namely, $V = E°(HBase^+/Base; H_2)$. Thus, we minimize χ^2 at this thermodynamic potential. As already said, the ΔG_k values are all linear functions of the three parameters $E°(Ni^{II/I})$, $E°(Ni^{I/0})$, and $pK_a(R'NH_3^+)$. Minimization of χ^2 yields the "optimum" catalyst under specific conditions. However, it should be noted

DOI: 10.1021/ar500342g
Acc. Chem. Res. 2015, 48, 248−255

that underlying the optimization are all of the steps included in the objective function, so verification is required in order to ensure that connected pathways that might act as thermodynamic sinks do not arise.

The outcome of the optimization is vividly illustrated in Figure 7, where the energy profiles for an existing catalyst (red)

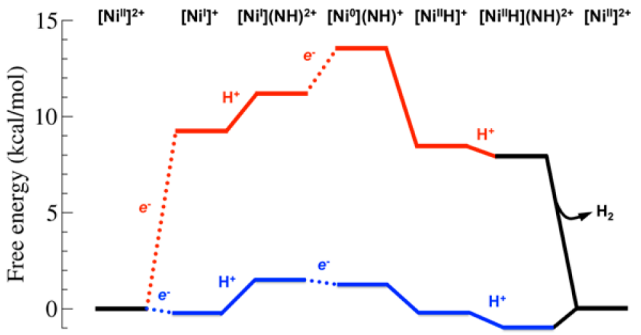

Figure 7. Free energy profiles for the EP^NEP^N pathway (see Figure 6) for H_2 production from $(DMF)H^+$ (pK_a = 6.1) as the exogenous acid in acetonitrile solution with the catalyst $[Ni(P^{Ph}{}_2N^{Ph}{}_2)_2]^{2+}$ (red) or the "optimum" catalyst based on eq 1 (blue). Free energies are given under standard conditions at 1 atm H_2 and the thermodynamic potential $V = E°((DMF)H^+/DMF; H_2)$.

and the "optimum" catalyst (blue) are displayed for comparison. We observe that for the "optimum" catalyst, the overpotential is close to zero by construction and the average free energy change per catalytic step is about 1.7 kcal/mol.

More generally, the result of the optimization is depicted in Figure 8: the top panel gives the "optimal" $E°(Ni^{II/I})$ (blue line) and $E°(Ni^{I/0})$ (red line) redox potentials as functions of the pK_a of the external acid; the bottom panel gives the "optimal" pK_a of the parent aminium. The optimal separation between $E°(Ni^{II/I})$ and $E°(Ni^{I/0})$ depends slightly on the strength of the external acid in the range of acidities of reaction media achievable in the laboratory, with a separation of ~0.51 V when $pK_a(HBase^+)$ = 0 and ~0.35 V when $pK_a(HBase^+)$ = 20. The values for catalysts synthesized to date are also displayed in Figure 8. It can be seen that the redox potentials for all of the existing H_2 production catalysts are too negative and that those for H_2 oxidation catalysts are too positive.

We can use Figure 8 to predict new synthetic targets. As an example, Figure 8 shows that with $(DMF)H^+$ as the external acid (pK_a = 6.1), the optimum catalyst should have $E°(Ni^{II/I})$ = −0.42 V, $E°(Ni^{I/0})$ = −0.88 V, and $pK_a(R'NH_3^+)$ = 11.6 (that of 4-methoxyaniline, i.e., *p*-anisidine, pK_a(*p*-anisidium) = 11.9). Accordingly, the optimum catalyst would have 4-methoxyphenyl groups as substituents on the pendant amines. $E°(Ni^{I/0})$ is controlled by the electronic properties of the substituents on P. The difference between the $E°(Ni^{II/I})$ and $E°(Ni^{I/0})$ redox potentials is controlled by the dihedral angle between the two diphosphine ligands in the four-coordinate $[Ni(P^R{}_2N^{R'}{}_2)_2]^{2+}$ complexes, which in turn is affected by steric interactions between the R substituents on these ligands.[15,17,37] The "optimal" $E°(Ni^{I/0})$ potential (−0.88 V) suggests that the catalyst should have substituents on the P atoms that are significantly more electron-withdrawing than a phenyl group. For $[Ni(P^{Ph}{}_2N^{Ph}{}_2)_2]^{2+}$, this potential is −1.02 V. In addition, the optimal difference in potentials between $E°(Ni^{II/I})$ and $E°(Ni^{I/0})$ ought to be ~0.46 V. This observation suggests that steric effects from R should be comparable to those from a

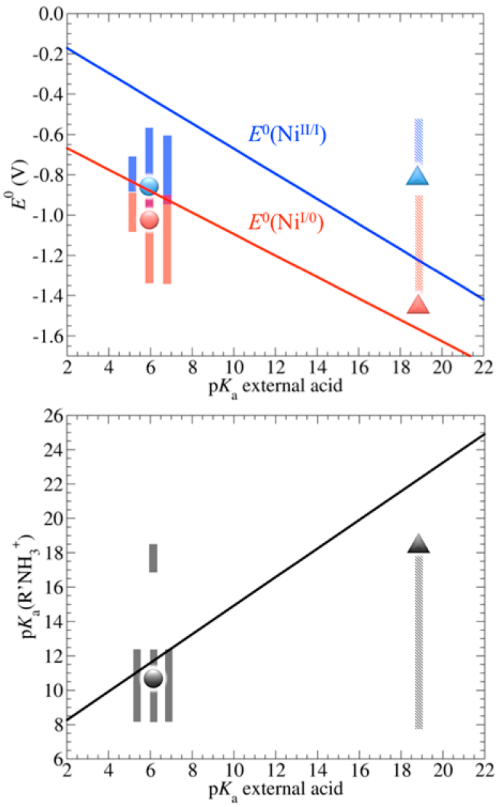

Figure 8. Optimal redox potentials $E°(Ni^{II/I})$ and $E°(Ni^{I/0})$ (top) and pK_a value of the parent aminium $pK_a(R'NH_3^+)$ (bottom) as functions of the pK_a of the external acid $HBase^+$ used for catalysis. Optimization was carried out at the thermodynamic potential $V = E°(HBase^+/Base; H_2)$. The ranges of values spanned by catalysts synthesized to date are displayed with solid bars (H_2 production) and shadowed bars (H_2 oxidation). Circles highlight specific values for the H_2 production catalyst $[Ni(P^{Ph}{}_2N^{Ph}{}_2)_2]^{2+}$ ($E°(Ni^{II/I})$ = −0.83 V, $E°(Ni^{I/0})$ = −1.02 V, $pK_a(PhNH_3^+)$ = 10.6) with $(DMF)H^+$ (pK_a = 6.1) as the external acid (the example in Figure 6). Triangles highlight specific values for the H_2 oxidation catalyst $[Ni(P^{Cy}{}_2N^{Bn}{}_2)_2]^{2+}$ ($E°(Ni^{II/I})$ = −0.45 V, $E°(Ni^{I/0})$ = −1.45 V, $pK_a(BnNH_3^+)$ = 18.4) with triethylamine as the external base ($pK_a(Et_3NH^+)$ = 18.8) in acetonitrile solution. Redox potentials are relative to the ferrocenium/ferrocene couple in acetonitrile.

cyclohexyl group, which leads to differences of ~0.5 V between $E°(Ni^{II/I})$ and $E°(^{I/0})$. We can rationalize this difference by considering the correlation between the $E°(Ni^{I/0})$ redox potential for a singly protonated (endo) complex and the $E°(Ni^{II/I})$ potential for the unprotonated complex shown in Scheme 7. The potentials for the two reduction steps in the catalytic cycle are now nearly the same.

The data reported in Figure 8 also show that it is not likely that efficient $[Ni(P^R{}_2N^{R'}{}_2)_2]^{2+}$ electrocatalysts operating with acids having a pK_a greater than 15 in acetonitrile can be designed. Indeed, Figure 8 indicates that beyond this acidity threshold of the reaction medium, the optimal catalyst would

Scheme 7. Expression for the $E°(Ni^{I/0})$ Redox Potential of a Singly-Protonated (Endo) Species; Compared with $E°(Ni^{I/0})$ of the Unprotonated Species, It Shows a Shift by a Constant Potential of 0.45 V and a Small Dependence on the Acidity of the Parent Aminium

$$E^0(Ni^{+/0})^{endo} = -0.006\ pK_a(\text{parent aminium}) + 0.91\ E^0(Ni^{+/0}) + 0.45$$

DOI: 10.1021/ar500342g
Acc. Chem. Res. 2015, 48, 248−255

originate from a parent aminium with pK_a > 19. To the best of our knowledge, primary amines with basicities that large are not available. Consequently, it is improbable to have efficient catalysts for H_2 oxidation operating with bases such as alkylamines. This consideration is clearly illustrated in Figure 8, which reports data points corresponding to $[Ni(P^{Cy}_2N^{Bn}_2)_2]^{2+}$ (Cy = cyclohexyl, Bn = benzyl), a Ni-based H_2 oxidation catalyst developed in our laboratory, with triethylamine as the external base (pK_a of the conjugated aminium = 18.8).

■ CONCLUSIONS AND PERSPECTIVE

The optimization analysis just described has its foundation on computation-driven linear free energy correlations. It is very powerful. We are in a position to suggest new synthetic targets with potentially enhanced efficiency. We must remark, however, that the objective function does not account for kinetic effects (activation barriers associated with individual steps along the catalytic pathway). Extension to account for kinetics will require further computations, possibly making use of Polanyi-like linear free energy relationships for activation barriers based on computed reaction free energies.

We have demonstrated to date that we know how to predict the "optimal" thermodynamic properties ($E°(Ni^{II/I})$, $E°(Ni^{I/0})$, and pK_a of the pendant amine) of efficient catalysts. At this point we are missing the knowledge to map these properties to actual first- and second-coordination-sphere substituents. What we know is that these thermodynamic properties depend on the electron-donating/withdrawing characteristics of the substituents and their steric effects on the catalyst structure (bite and twist angles that affect the redox potentials). This mapping should be achievable through computed Taft-like relations[9] linking chemical composition and electronic and steric effects. Such an analysis is in progress.

■ AUTHOR INFORMATION

Corresponding Authors

*simone.raugei@pnnl.gov (S.R.)
*roger.rousseau@pnnl.gov (R.R.)
*michel.dupuis@pnnl.gov (M.D.)

Author Contributions

The manuscript was written through contributions of all authors.

Funding

This research was carried out at the Center for Molecular Electrocatalysis, an Energy Frontier Research Center funded by the U.S. Department of Energy (DOE), Office of Science, Office of Basic Energy Sciences. Pacific Northwest National Laboratory (PNNL) is operated for the DOE by Battelle. Computer resources were provided by the W. R. Wiley Environmental Molecular Sciences Laboratory (EMSL), a National Scientific User Facility located at PNNL and sponsored by DOE's Office of Biological and Environmental Research. Computer resources were also provided by the National Energy Research Computing Center (NERSC) at the Lawrence Berkeley National Laboratory.

Notes

The authors declare no competing financial interest.

Biographies

Simone Raugei obtained a Ph.D. in Theoretical Chemistry at the University of Florence in 2000. He was an Assistant Professor of Biophysics at the International School for Advanced Studies (SISSA) in Trieste from 2002 to 2009. He has been a Senior Scientist at Pacific Northwest National Laboratory (PNNL) since 2010. His research deals with computation and modeling of chemical and biochemical processes for energy storage and energy delivery.

Daniel L. DuBois received a Ph.D. at The Ohio State University in 1975. He was a Principal Scientist at National Renewable Energy Laboratory from 1981 to 2005 and a Laboratory Fellow at PNNL from 2006 to 2014. His research interests include catalytic interconversion of fuels and electricity, synthetic organometallic and inorganic chemistry, thermodynamics relevant to catalysis, and the role of proton relays in electrocatalytic reactions.

Roger Rousseau obtained a Ph.D. at the University of Michigan in 1995. He was an Associate Professor of Condensed Matter Physics at SISSA from 2004 to 2007. He is a senior scientist at PNNL's Institute for Integrated Catalysis. His research deals with application and development of ab initio molecular dynamics for catalysis.

Shentan Chen obtained a Ph.D. at The Ohio State University in 2009. He was a postdoctoral fellow at the Center for Molecular Electrocatalysis at PNNL from 2009 to 2013. He joined the group of Prof. Musaev at Emory University in 2013. His research deals with theoretical studies of transition-metal complexes with applications to electrochemistry, catalysis, and materials science.

Ming-Hsun Ho obtained a Ph.D. at the University of Pennsylvania in 2010. He was a postdoctoral fellow at the Center for Molecular Electrocatalysis at PNNL from 2010 to 2013. In 2013, he moved to Shanghai Hengrui Pharmaceuticals, where he is a scientist in the Department of Computational Chemistry.

R. Morris Bullock obtained a Ph.D. at the University of Wisconsin. He was at Brookhaven National Laboratory from 1985 to 2006, where his research focused on reactions of transition-metal hydride complexes. He is a Laboratory Fellow at PNNL and the Director of the Center for Molecular Electrocatalysis.

Michel Dupuis obtained a Ph.D. at the University of Buffalo in 1976. Over the years he has contributed to the development of quantum-chemical codes (HONDO, GAMESS, and NWChem). He has been a Laboratory Fellow at PNNL since 1995, and his research focuses on computation and simulation for new energy technologies.

■ ACKNOWLEDGMENTS

We acknowledge stimulating discussions with Dr. Aaron Appel (PNNL). We also sincerely thank Dr. Jon Darmon (PNNL) for the Conspectus graphics.

■ ABBREVIATIONS

DFT, density functional theory; pK_a, acidity constant; $E°$, redox potential; ΔG_{H^-}, hydride donor ability

■ REFERENCES

(1) DuBois, D. L. Development of Molecular Electrocatalysts for Energy Storage. *Inorg. Chem.* **2014**, *53*, 3935−3960.
(2) Pople, J. A.; Head-Gordon, M.; Fox, D. J.; Raghavachari, K.; Curtiss, L. A. Gaussian-1 Theory: A General Procedure for Prediction of Molecular Energies. *J. Chem. Phys.* **1989**, *90*, 5622−5629.
(3) Peterson, K. A.; Feller, D.; Dixon, D. A. Chemical Accuracy in Ab Initio Thermochemistry and Spectroscopy: Current Strategies and Future Challenges. *Theor. Chem. Acc.* **2012**, *131*, 1079.

DOI: 10.1021/ar500342g
Acc. Chem. Res. 2015, 48, 248−255

(4) Ruscic, B. Uncertainty Quantification in Thermochemistry, Benchmarking Electronic Structure Computations, and Active Thermochemical Tables. *Int. J. Quantum Chem.* **2014**, *114*, 1097−1101.
(5) Chen, S.; Rousseau, R.; Raugei, S.; Dupuis, M.; DuBois, D. L.; Bullock, R. M. Comprehensive Thermodynamics of Nickel Hydride Bis(diphosphine) Complexes: A Predictive Model through Computations. *Organometallics* **2011**, *30*, 6108−6118.
(6) Chen, S.; Ho, M.-H.; Bullock, R. M.; DuBois, D. L.; Dupuis, M.; Rousseau, R.; Raugei, S. Computing Free Energy Landscapes: Application to Ni-Based Electrocatalysts with Pendant Amines for H_2 Production and Oxidation. *ACS Catal.* **2014**, *4*, 229−242.
(7) Roberts, J. A. S.; Bullock, R. M. Direct Determination of Equilibrium Potentials for Hydrogen Oxidation/Production by Open Circuit Potential Measurements in Acetonitrile. *Inorg. Chem.* **2013**, *52*, 3823−3835.
(8) Appel, A. M.; Helm, M. L. Determining the Overpotential for a Molecular Electrocatalyst. *ACS Catal.* **2014**, *4*, 630−633.
(9) Taft, R. W., Jr. Linear Free Energy Relationships from Rates of Esterification and Hydrolysis of Aliphatic and Ortho-Substituted Benzoate Esters. *J. Am. Chem. Soc.* **1952**, *74*, 2729−2732.
(10) Friedman, D.; Masciangioli, T.; Olson, S. *The Role of the Chemical Sciences in Finding Alternatives to Critical Resources: A Workshop Summary*; National Academies Press: Washington, DC, 2012.
(11) Bullock, R. M. *Catalysis without Precious Metals*; Wiley-VCH: Weinheim, Germany, 2010.
(12) Cook, T. R.; Dogutan, D. K.; Reece, S. Y.; Surendranath, Y.; Teets, T. S.; Nocera, D. G. Solar Energy Supply and Storage for the Legacy and Nonlegacy Worlds. *Chem. Rev.* **2010**, *110*, 6474−6502.
(13) Lewis, N. S.; Nocera, D. G. Powering the Planet: Chemical Challenges in Solar Energy Utilization. *Proc. Natl. Acad. Sci. U.S.A.* **2006**, *103*, 15729−15735.
(14) Tran, P. D.; Artero, V.; Fontecave, M. Water Electrolysis and Photoelectrolysis on Electrodes Engineered Using Biological and Bio-Inspired Molecular Systems. *Energy Environ. Sci.* **2010**, *3*, 727−747.
(15) DuBois, M. R.; DuBois, D. L. The Roles of the First and Second Coordination Spheres in the Design of Molecular Catalysts for H_2 Production and Oxidation. *Chem. Soc. Rev.* **2009**, *38*, 62−72.
(16) Wayner, D. D. M.; Parker, V. D. Bond Energies in Solution from Electrode Potentials and Thermochemical Cycles. A Simplified and General Approach. *Acc. Chem. Res.* **1993**, *26*, 287−294.
(17) Berning, D. E.; Miedaner, A.; Curtis, C. J.; Noll, B. C.; Rakowski DuBois, M. C.; DuBois, D. L. Free-Energy Relationships between the Proton and Hydride Donor Abilities of $[HNi(diphosphine)_2]^+$ Complexes and the Half-Wave Potentials of Their Conjugate Bases. *Organometallics* **2001**, *20*, 1832−1839.
(18) Wang, D.; Angelici, R. J. Metal−Hydrogen Bond Dissociation Enthalpies in Series of Complexes of Eight Different Transition Metals. *J. Am. Chem. Soc.* **1996**, *118*, 935−942.
(19) Simoes, J. M.; Beauchamp, J. L. Transition Metal−Hydrogen and Metal−Carbon Bond Strengths: The Keys to Catalysis. *Chem. Rev.* **1990**, *90*, 629−688.
(20) Parker, V. D.; Handoo, K. L.; Roness, F.; Tilset, M. Electrode Potentials and the Thermodynamics of Isodesmic Reactions. *J. Am. Chem. Soc.* **1991**, *113*, 7493−7498.
(21) Dedieu, A. *Transition Metal Hydrides*; VCH: Weinheim, Germany, 1992.
(22) O'Hagan, M.; Shaw, W. J.; Raugei, S.; Chen, S.; Yang, J. Y.; Kilgore, U. J.; DuBois, D. L.; Bullock, R. M. Moving Protons with Pendant Amines: Proton Mobility in a Nickel Catalyst for Oxidation of Hydrogen. *J. Am. Chem. Soc.* **2011**, *133*, 14301−14312.
(23) O'Hagan, M.; Ho, M.-H.; Yang, J. Y.; Appel, A. M.; DuBois, M. R.; Raugei, S.; Shaw, W. J.; DuBois, D. L.; Bullock, R. M. Proton Delivery and Removal in $[Ni(P^R_2N^{R'}_2)_2]^{2+}$ Hydrogen Production and Oxidation Catalysts. *J. Am. Chem. Soc.* **2012**, *134*, 19409−19424.
(24) Raugei, S.; Chen, S.; Ho, M.-H.; Ginovska-Pangovska, B.; Rousseau, R. J.; Dupuis, M.; DuBois, D. L.; Bullock, R. M. The Role of Pendant Amines in the Breaking and Forming of Molecular Hydrogen Catalyzed by Nickel Complexes. *Chem.—Eur. J.* **2012**, *18*, 6493−6506.
(25) Carver, C. T.; Matson, B. D.; Mayer, J. M. Electrocatalytic Oxygen Reduction by Iron Tetra-arylporphyrins Bearing Pendant Proton Relays. *J. Am. Chem. Soc.* **2012**, *134*, 5444−5447.
(26) Matson, B. D.; Carver, C. T.; Von Ruden, A.; Yang, J. Y.; Raugei, S.; Mayer, J. M. Distant Protonated Pyridine Groups in Water-Soluble Iron Porphyrin Electrocatalysts Promote Selective Oxygen Reduction to Water. *Chem. Commun.* **2012**, *48*, 11100−11102.
(27) Wiedner, E. S.; Appel, A. M. Thermochemical Insight into the Reduction of CO to CH_3OH with $[Re(CO)]^+$ and $[Mn(CO)]^+$ Complexes. *J. Am. Chem. Soc.* **2014**, *136*, 8661−8668.
(28) Solis, B. H.; Hammes-Schiffer, S. Proton-Coupled Electron Transfer in Molecular Electrocatalysis: Theoretical Methods and Design Principles. *Inorg. Chem.* **2014**, *53*, 6427−6443.
(29) DuBois, D. L.; Bullock, R. M. Molecular Electrocatalysts for the Oxidation of Hydrogen and the Production of Hydrogen—The Role of Pendant Amines as Proton Relays. *Eur. J. Inorg. Chem.* **2011**, 1017−1027.
(30) Mock, M. T.; Potter, R. G.; Camaioni, D. M.; Li, J.; Dougherty, W. G.; Kassel, W. S.; Twamley, B.; DuBois, D. L. Thermodynamic Studies and Hydride Transfer Reactions from a Rhodium Complex to BX_3 Compounds. *J. Am. Chem. Soc.* **2009**, *131*, 14454−14465.
(31) Mock, M. T.; Potter, R. G.; O'Hagan, M. J.; Camaioni, D. M.; Dougherty, W. G.; Kassel, W. S.; DuBois, D. L. Synthesis and Hydride Transfer Reactions of Cobalt and Nickel Hydride Complexes to BX_3 Compounds. *Inorg. Chem.* **2011**, *50*, 11914−11928.
(32) DuBois, D. L.; Blake, D. M.; Miedaner, A.; Curtis, C. J.; DuBois, M. R.; Franz, J. A.; Linehan, J. C. Hydride Transfer from Rhodium Complexes to Triethylborane. *Organometallics* **2006**, *25*, 4414−4419.
(33) Qi, X.-J.; Fu, Y.; Liu, L.; Guo, Q.-X. Ab Initio Calculations of Thermodynamic Hydricities of Transition-Metal Hydrides in Acetonitrile. *Organometallics* **2007**, *26*, 4197−4203.
(34) Qi, X.-J.; Liu, L.; Fu, Y.; Guo, Q.-X. Ab Initio Calculations of pK_a Values of Transition-Metal Hydrides in Acetonitrile. *Organometallics* **2006**, *25*, 5879−5886.
(35) Chen, S.; Raugei, S.; Rousseau, R.; Dupuis, M.; Bullock, R. M. Homogeneous Ni Catalysts for H_2 Oxidation and Production: An Assessment of Theoretical Methods, from Density Functional Theory to Post Hartree−Fock Correlated Wave-Function Theory. *J. Phys. Chem. A* **2010**, *114*, 12716−12724.
(36) Hehre, W. J.; Ditchfield, R.; Radom, L.; Pople, J. A. Molecular Orbital Theory of the Electronic Structure of Organic Compounds. V. Molecular Theory of Bond Separation. *J. Am. Chem. Soc.* **1970**, *92*, 4796−4801.
(37) Miedaner, A.; Haltiwanger, R. C.; DuBois, D. L. Relationship between the Bite Size of Diphosphine Ligands and Tetrahedral Distortions of "Square-Planar" Nickel(II) Complexes: Stabilization of Nickel(I) and Palladium(I) Complexes Using Diphosphine Ligands with Large Bites. *Inorg. Chem.* **1991**, *30*, 417−427.
(38) Hammes-Schiffer, S.; Soudackov, A. V. Proton-Coupled Electron Transfer in Solution, Proteins, and Electrochemistry. *J. Phys. Chem. B* **2008**, *112*, 14108−14123.
(39) Warren, J. J.; Tronic, T. A.; Mayer, J. M. Thermochemistry of Proton-Coupled Electron Transfer Reagents and Its Implications. *Chem. Rev.* **2010**, *110*, 6961−7001.
(40) Kilgore, U. J.; Roberts, J. A. S.; Pool, D. H.; Appel, A. M.; Stewart, M. P.; DuBois, M. R.; Dougherty, W. G.; Kassel, W. S.; Bullock, R. M.; DuBois, D. L. $[Ni(P^{Ph}_2N^{C_6H_4X}_2)_2]^{2+}$ Complexes as Electrocatalysts for H_2 Production: Effect of Substituents, Acids, and Water on Catalytic Rates. *J. Am. Chem. Soc.* **2011**, *133*, 5861−5872.
(41) Kilgore, U. J.; Stewart, M. P.; Helm, M. L.; Dougherty, W. G.; Kassel, W. S.; DuBois, M. R.; DuBois, D. L.; Bullock, R. M. Studies of a Series of $[Ni(P^R_2N^{Ph}_2)_2(CH_3CN)]^{2+}$ Complexes as Electrocatalysts for H_2 Production: Substituent Variation at the Phosphorus Atom of the P_2N_2 Ligand. *Inorg. Chem.* **2011**, *50*, 10908−10918.

DOI: 10.1021/ar500342g
Acc. Chem. Res. 2015, 48, 248−255